TU/e EINDHOVEN UNIVERSITY OF TECHNOLOGY

Thermo-mechanically coupled modelling of a single-asperity scratch on an isotropic isotactic polypropylene surface

Citation for published version (APA):
Kershah, T., Looijmans, S., Anderson, P., & van Breemen, L. (2020). Thermo-mechanically coupled modelling of a single-asperity scratch on an isotropic isotactic polypropylene surface. *Tribology International*, *141*, Article 105946. https://doi.org/10.1016/j.triboint.2019.105946

Document license:
CC BY-NC-ND

DOI:
10.1016/j.triboint.2019.105946

Document status and date:
Published: 01/01/2020

Document Version:
Publisher's PDF, also known as Version of Record (includes final page, issue and volume numbers)

Please check the document version of this publication:

• A submitted manuscript is the version of the article upon submission and before peer-review. There can be important differences between the submitted version and the official published version of record. People interested in the research are advised to contact the author for the final version of the publication, or visit the DOI to the publisher's website.
• The final author version and the galley proof are versions of the publication after peer review.
• The final published version features the final layout of the paper including the volume, issue and page numbers.

Link to publication

General rights
Copyright and moral rights for the publications made accessible in the public portal are retained by the authors and/or other copyright owners and it is a condition of accessing publications that users recognise and abide by the legal requirements associated with these rights.

• Users may download and print one copy of any publication from the public portal for the purpose of private study or research.
• You may not further distribute the material or use it for any profit-making activity or commercial gain
• You may freely distribute the URL identifying the publication in the public portal.

If the publication is distributed under the terms of Article 25fa of the Dutch Copyright Act, indicated by the "Taverne" license above, please follow below link for the End User Agreement:

www.tue.nl/taverne

Take down policy
If you believe that this document breaches copyright please contact us at:

openaccess@tue.nl

providing details and we will investigate your claim.

Download date: 16. Nov. 2023

Tribology International 141 (2020) 105946

Contents lists available at ScienceDirect

Tribology International

journal homepage: http://www.elsevier.com/locate/triboint

Thermo-mechanically coupled modelling of a single-asperity scratch on an isotropic isotactic polypropylene surface

Tarek Kershah [a,b], Stan F.S.P. Looijmans [a,b], Patrick D. Anderson [a], Lambèrt C.A. van Breemen [a,*]

[a] Polymer Technology, Department of Mechanical Engineering, Materials Technology Institute, Eindhoven University of Technology, P.O. Box 513, 5600 MB, Eindhoven, the Netherlands
[b] Dutch Polymer Institute (DPI), P.O. Box 902, 5600 AX, Eindhoven, the Netherlands

ARTICLE INFO

Keywords:
Contact mechanics
Single-asperity sliding friction
Finite element modelling
Thermomechanical analysis

ABSTRACT

Isotactic polypropylene (iPP) is a low cost semi-crystalline polymer that is easy to process, has a wide variety in properties and is, therefore, used in many applications. Many of these applications require enhanced wear-resistance to prolong the lifetime of the product. Essential is to first investigate the intrinsic response of the material in order to describe its friction and wear response. In this respect, a hybrid experimental-numerical approach is used to couple the intrinsic response to the single-asperity scratch response. The numerical model used is a 3D elasto-viscoplastic model based on the Eindhoven Glassy Polymer (EGP) model. For the first time a coupled thermo-mechanical EGP model is implemented in a Finite Element Method (FEM)-framework. The model is capable of accurately describing the intrinsic response of the material, which opens the door to qualitatively and quantitatively describe its frictional response and understand the damage formation mechanism (i.e. the initiation of wear). In this study, α- and β-phase iPP are studied. We show that the difference in the intrinsic response between the two phases has a significant influence on the friction and wear response. Moreover, a stick-slip phenomenon is proven to be the main responsible for the damage mechanism observed. The observed periodic "fish-scale" damage pattern results from periodic changes in resistance during the tip movement. A relation between the polymer intrinsic response and the damage formation mechanism is established. The influence of the applied load and scratch speed on damage formation is investigated as well.

1. Introduction

Nowadays, semi-crystalline polymers are used in many applications where moving parts are in contact. The reason is that semi-crystalline polymers possess excellent physical properties such as a light weight and a high wear resistance. Polymers are favoured above their metal counterparts in many applications such as artificial joints, gears, and bearings.

The background of this study is the methodology developed in our group over last two decades where numerical simulations are combined with experiments in order to link the intrinsic behaviour of the polymer to its frictional response. The constitutive model framework used is the Eindhoven Glassy Polymer (EGP) model [1–6], which, like the Boyce-Parks-Argon model [7,8] and the Oxford Glass-Rubber (OGR) model [9–11] accurately describes the deformation kinetics of glassy polymers. The constitutive model was extended to better capture the non-linear visco-elastic response (multi-mode) [12,13] and the thermorheological complex systems (multi-process) [5]. Recently, Van Breemen et al. [14] and Krop et al. [15] used the EGP model to couple intrinsic material properties to the observed frictional response on both unfilled and particle-filled polycarbonate. In practice however, for example in bearing cages and medical implants such as knee or hip replacements, semi-crystalline polymers are used [16–20]. Generally speaking, semi-crystalline polymers exhibit high strength, better wear and chemical resistance than glassy polymers.

Semi-crystalline polymers have a large variety of morphological structures. Therefore, contrary to glassy polymers, semi-crystalline systems display a large variation in mechanical properties and lifetime depending on for instance the cooling rate, applied pressure, and presence of anisotropy [21]. We chose isotactic polypropylene (iPP) as a model material since it is one of the widely used semi-crystalline polymers, in addition to its well-defined mechanical properties [22–26].

In this study we aim to link the intrinsic material behaviour to the observed friction and wear response, and obtain a comprehensive

* Corresponding author.
E-mail address: L.C.A.v.Breemen@tue.nl (L.C.A. van Breemen).

https://doi.org/10.1016/j.triboint.2019.105946
Received 12 July 2019; Received in revised form 30 August 2019; Accepted 31 August 2019
Available online 5 September 2019
0301-679X/© 2019 The Authors. Published by Elsevier Ltd. This is an open access article under the CC BY-NC-ND license (http://creativecommons.org/licenses/by-nc-nd/4.0/).

understanding of the influence of intrinsic response on macroscopic deformation, frictional energy loss, and damage mechanism using single-asperity scratching simulations. Single-asperity scratch simulations have been previously used to simulate the damage formation on polypropylene surface [27]. In addition, Looijmans et al. [28] experimentally investigated the effect of pre-stretch on the frictional response of iPP using single-asperity scratch with a rigid diamond indenter. However, a solid link between the intrinsic response of the polymer and its scratch and frictional response has never been established. A key aspect in this study is the thermo-mechanically coupled modelling that is introduced into the EGP model and implemented in a Finite Element Method (FEM)-framework for the first time. The reason is, like metals, a percentage of the mechanical work of polymers has been found to be dissipative, in other words, heat is generated due to plastic deformation [29,30]. The thermal model is analogue to the work of Boyce et al. [30] and Klompen et al. [31]. It is used to first quantitatively investigate the material intrinsic response, and help predict the material frictional response. An additional important aspect is the significant difference in strain hardening between the intrinsic response of α and β-phase iPP. It has been previously shown that strain hardening plays a determining role in strain localization [32,33]. Strain hardening stabilizes the deformation zones and resists the formation of localized plastic deformation zones. In this respect, we expect to see a different frictional response between the two phases of iPP. In addition, we aim to understand the damage formation mechanism of iPP (i.e. the initiation of wear). It has been shown previously that a stick-slip phenomenon plays a major part in the damage formation mechanism of iPP [34]. The gradual build-up of friction force during sticking, and the sudden drop during slipping results in the so-called fish-scale damage pattern by plastically drawing the material along the scratch direction [35–37]. The intrinsic response of the polymer must have an influence on such a mechanism. Moreover, the normal load and scratching speed significantly affect the stick–slip process of the polymer, and thus, influence the damage-formation mechanism. The sample preparation and nano indentation testing procedures are discussed in Section 2. The detailed description of the EGP constitutive model and its extension to a thermo-mechanically coupled model is discussed in Section 3. In the same section the FEM scratch model is also demonstrated. In the results section we compare numerical simulations with the experimental results to study the damage formation and the parameters influencing it.

2. Experimental

2.1. Materials and sample preparation

An injection moulding grade iPP homopolymer with weight-averaged molar mass M_w of 320 kg/mol and polydispersity M_w/M_n of 5.4 is kindly provided by SABIC (Riyad, Saudi Arabia). This particular grade was selected because the intrinsic deformation kinetics of its main crystal phases are well-characterized by Caelers et al. [26]. Compression response data is adopted from this work. Experimental data regarding the scratch response of α-phase iPP is adopted from a previous work [28]. Polymer granules are molten at 230 °C and manually compressed between glass slides to ensure a smooth surface with respect to the indenter geometry. Polymer films of approximately 500 μm in thickness, are kept isothermal in the melt for 10 min to erase thermomechanical history and subsequently cooled to room temperature. Using this procedure, α-phase samples with a crystallinity of about 61% are obtained. Analogously, β-phase samples are prepared from granules containing 0.1 wt% β-nucleating agent (NJSTAR NU100 New Japan Chemical Group). The exact compounding procedure of this material can be found elsewhere [25]. Samples having a volumetric crystallinity of 64% were obtained, using the thermal protocol described above.

2.2. Sliding friction experiments

An MTS Nano Indenter XP is used to perform scratch test experiments by sliding a conical, diamond indenter tip (cone angle 90°, top radius 50 μm) over the smooth polymer surface. The normal load applied to indenter geometry, as well as the sliding velocity, are kept constant during a single sliding friction experiment. Normal loads are varied between 200 and 400 mN at sliding velocities ranging from 1 till 100 μm/s. The penetration depth and lateral force are recorded as function of sliding distance. To ensure steady-state measurements, scratch tests of 1 mm in length are performed. At each combination of applied load and sliding velocity, the scratch response is measured three times to check for reproducibility.

3. Constitutive modelling

3.1. The EGP model for thermorheologically simple polymers

The 3D elasto-viscoplastic constitutive model used, see Van Breemen et al. [13] for more details, consists of multiple Maxwell elements connected in parallel to a neo-Hookean spring. In the model the total stress $\boldsymbol{\sigma}$ is split into the driving stress $\boldsymbol{\sigma}_s$ and the hardening stress $\boldsymbol{\sigma}_r$:

$$\boldsymbol{\sigma} = \boldsymbol{\sigma}_s + \boldsymbol{\sigma}_r. \tag{1}$$

Physically, the hardening stress is interpreted as a rubber elastic contribution of the entangled network. Mathematically, it is described with a simple neo-Hookean relation:

$$\boldsymbol{\sigma}_r = \frac{G_r}{J}\tilde{\boldsymbol{B}}^d, \tag{2}$$

herein, G_r denotes the hardening modulus, $\tilde{\boldsymbol{B}}^d$ is the deviatoric part of the isochoric left Cauchy-Green strain tensor, and J is the volume change ratio. The driving stress is attributed to intermolecular interactions [3,12] and is split into a hydrostatic and a deviatoric part [1]:

$$\boldsymbol{\sigma}_s = \boldsymbol{\sigma}_s^h + \boldsymbol{\sigma}_s^d = \kappa(J-1)\boldsymbol{I} + \sum_{i=1}^{n} G_i \tilde{\boldsymbol{B}}_{e,i}^d, \tag{3}$$

where, κ is the bulk modulus, G is the shear modulus, $\tilde{\boldsymbol{B}}_e^d$ is the elastic deviatoric part of the isochoric left Cauchy-Green strain tensor. The subscript i refers to a specific mode, and n denotes the number of modes [13]. The plastic deformation-rate tensor $\boldsymbol{D}_p$ is related to the deviatoric stress $\boldsymbol{\sigma}_s^d$ via a non-Newtonian flow rule:

$$\boldsymbol{D}_{p,i} = \frac{\boldsymbol{\sigma}_{s,i}^d}{2\eta_i}, \tag{4}$$

where η_i are the viscosities of each Maxwell element which are described by the extended Eyring flow rule. This flow rule was extended [2,38–40] to take the pressure dependence and strain softening into account:

$$\eta_i = \eta_{0,\mathrm{ref},i}\frac{\bar{\tau}/\tau_0}{\sinh(\bar{\tau}/\tau_0)}\exp\left[\frac{\mu p}{\tau_0}\right]\exp\left[S_a R_x(\bar{\gamma}_p)\right], \tag{5}$$

where $\eta_{0,\mathrm{ref},i}$ is the reference viscosity of each Maxwell element, $\bar{\tau}$ is the total equivalent stress, τ_0 defines the characteristic shear stress, p is the hydrostatic pressure, the pressure dependency is governed by the parameter μ, the physical ageing is contained in the state parameter S_a. The softening function $R_x(\bar{\gamma}_p)$ describes the strain-softening process, i.e. the erasure of thermal history upon the inception of plastic deformation. Klompen et al. [3] expressed $R_x(\bar{\gamma}_p)$ as a function of $\bar{\gamma}_p$ using a modified Carreau-Yasuda relation:

$$R_x(\bar{\gamma}_p) = \left[\frac{1+\left(r_0.\exp(\bar{\gamma}_p)\right)^{r_1}}{1+r_0^{r_1}}\right]^{(r_2-1)/r_1}, \tag{6}$$

where $\bar{\gamma}_p$ is the equivalent plastic strain, and r_0, r_1, and r_2 are the fitting parameters.

When temperature is considered, a temperature-dependent pre-exponential factor is added to the Eyring equation:

$$\eta_i = \eta_{0,\mathrm{ref},i}\frac{\bar{\tau}/\tau_0}{\sinh(\bar{\tau}/\tau_0)}\exp\left[\frac{\mu p}{\tau_0}\right]\exp\left[S_a R_x(\bar{\gamma}_p)\right]\exp\left[-\frac{\Delta U}{RT}\left(\frac{T-T_{\mathrm{ref}}}{T_{\mathrm{ref}}}\right)\right], \tag{7}$$

where ΔU is the activation energy, R is the universal gas constant, T represents the temperature, and T_{ref} is the room temperature. In addition, τ_0 is determined using the following equation:

$$\tau_0 = \frac{kT}{V^*}, \tag{8}$$

where k is the Boltzman's constant and V^* is the activation volume.

3.2. Extension to thermorheologically complex behaviour

The experimental findings of Van Breemen et al. [5] clearly show the existence of a secondary molecular process in iPP as it has been tested over broad range of strain rates. This thermorheologically complex behaviour contributes to an increased strain-rate dependency of the polymer at high strain rates. To capture this complex behaviour of the polymer we use a straightforward extension of Equation (1) based on the Ree-Eyring equation [41]:

$$\boldsymbol{\sigma} = \boldsymbol{\sigma}_{s,1} + \boldsymbol{\sigma}_{s,2} + \boldsymbol{\sigma}_r, \tag{9}$$

where $\boldsymbol{\sigma}_{s,1}$ is the driving stress of the primary process ($\boldsymbol{\sigma}_s$ in Equation (3)), and $\boldsymbol{\sigma}_{s,2}$ is the driving stress for the secondary process. Both stresses have their own temperature and rate dependencies. Therefore, each process has its own characteristic values of the activation volume V^* and activation energy ΔU. In comparison to experimental data, Equation (9) has been shown to be effective in capturing the response of many polymers including iPP [42].

3.3. Extension to thermo-mechanically coupled model

A thermo-mechanically coupled model must be used if deformation converts mechanical work into heat through an irreversible process which cannot be neglected relative to other heat sources [43–45]. For metals the amount of dissipated energy is approximately 90–95% [30]. Adams et al. [29] showed that around 50%–80% of the work of deformation is dissipated into heat during cold drawing of polycarbonate. Therefore, in case of applying relatively high deformation rates, it becomes a necessity to use a thermo-mechanically coupled model in order to capture the intrinsic response of the polymer. The model is formulated analogous to Boyce et al. [30]. The general energy balance equation of a 3D system is given by:

$$\rho c_p \dot{T} = -\nabla\cdot\boldsymbol{q} + \dot{Q}_d, \tag{10}$$

where the left hand side represents the rate of change in the internal heat energy per unit volume in the material with ρ being the material density and c_p the specific heat capacity. In the first part of the right hand side, the Operator ∇ acts as the divergence operator, and the vector $\boldsymbol{q} = \boldsymbol{q}\{\boldsymbol{x}, t\}$ is a vector field that represents the magnitude and the direction of the heat flow at the point $\boldsymbol{x}$ of space and time t. This vector is given by Fourier's law for an isotropic homogeneous medium where the rate of flow of heat energy per unit volume through a surface is proportional to the negative temperature gradient across it:

$$\boldsymbol{q} = -k_p\nabla T, \tag{11}$$

where k_p is the proportionality coefficient which represents the polymer thermal conductivity. The second part of the right hand side, $\dot{Q}_d$, is the rate of change in the dissipative work done by the driving stress given by:

$$\dot{Q}_d = \Gamma\left(\boldsymbol{\sigma}_s : \boldsymbol{D}_{p,i}\right), \tag{12}$$

where Γ is the percentage of mechanical work dissipated into heat. This percentage gradually decreases as the material continues to be strained due to extensive molecular orientation [30].

Next, the boundary conditions should be considered. In compression experiments, steel compression plates are used to compress the sample, while in scratch experiments, the indenter comes in contact with the polymer. In that respect, the change in the heat flux due to the conduction boundary condition is given by:

$$\dot{Q}_a = A_a(k_a/t_a)\left(T - T_{\mathrm{ref}}\right), \tag{13}$$

where A_a is the contact area between the sample and the steel compression plates in the compression test or the indenter in the scratch test, k_a and t_a are the thermal conductivity and the thickness of the body in contact with the polymer. Similarly heat convection to the surrounding air must be considered, it is given by the following relation:

$$\dot{Q}_c = A_c h_c\left(T - T_{\mathrm{ref}}\right), \tag{14}$$

where A_c is the contact area between the sample and the air, h_c is the heat transfer coefficient of the air. Radiation effects are very small and, therefore, neglected. Since the thermal conductivity of polymers k_p is relatively small and the volume of the surrounding contact bodies are relatively large with respect to the sample, the surrounding mediums are considered as heat sinks. Therefore, the heat transfer within the polymer will be neglected. Similar to Ref. [31], the boundary conditions parts are added to Equation (10). The equation of evolution can be written as follows:

$$\dot{T} = \frac{1}{\rho c_p}\left[\Gamma\left(\boldsymbol{\sigma}_s : \boldsymbol{D}_{p,i}\right) - \left[(A_c h_c) + A_a(k_a/t_a)\right]\left(T - T_{\mathrm{ref}}\right)\right]. \tag{15}$$

it is difficult to quantitatively determine the boundary conditions parameters, they are also different for different tests, i.e. compression or scratch. In that respect, a boundary condition parameter k is used instead and is determined by fitting the simulation results to the experimental compression data. For simplicity the same value of k will be used in the scratch simulations. This parameter encompasses all the boundary condition parameters in addition to the thermal conductivity and heat transfer coefficient of the mediums which are in contact with the polymer. The final evolution equation is given by:

$$\dot{T} = \frac{1}{\rho c_p}\left[\Gamma\left(\boldsymbol{\sigma}_s : \boldsymbol{D}_{p,i}\right) - k\left(T - T_{\mathrm{ref}}\right)\right]. \tag{16}$$

The evolution equation is then solved using the forward Euler method:

$$T_c = T_b + \Delta t\dot{T}, \tag{17}$$

where T_c is the nodal temperature of the current increment, T_b is the temperature of the previous increment, and Δt is the incremental time step.

3.4. Friction modelling and FEM mesh

The constitutive model is implemented in the FEM package MSC. Marc in order to simulate the single-asperity scratch test. The Coulomb model is adopted as a friction model. The arctangent model is used to avoid the numerical singularities by smoothening the stick-slip transition, similar to Refs. [14,15]:

$$\boldsymbol{f}_t = -\mu_f f_n\frac{2}{\pi}\arctan\left[\frac{|\mathbf{v}_r|}{\delta}\right]\boldsymbol{t}, \tag{18}$$

where $\boldsymbol{f}_t$ and f_n are the friction and normal forces respectively, μ_f the

local friction coefficient, v_r is the relative sliding velocity, and t is the tangential vector. The value of δ determines the value of the relative velocity below which sticking occurs. A large value of δ will guarantee quick convergence but poor estimation of the friction force. A small value will result in better estimation of the friction force at the cost of more computational power, and, if too small, it will be impossible to reach convergence. Many simulations have been used to optimize this parameter. The friction coefficient μ_f is determined by fitting the simulations frictional response to experimental data in a fashion similar to Van Breemen et al. [14]. A local friction coefficient value of $\mu_f = 0.28$ is found to give the best description of the experimental scratching data of both iPP phases.

The single-asperity scratch mesh is shown in Fig. 1a. Only half of the polymer surface is meshed since the simulation is symmetric. The meshed volume is $0.2 \times 0.2 \times 0.8\,mm^3$. The symmetry plane is fixed in y-direction and the sides are restrained in x- and z-direction. Room temperature is used as an initial condition at each node. An indenter with a tip radius 50 μm is used, and is modelled as a rigid body. Mesh refinement is applied to the area of greatest interest, i.e. largest deformation. Fig. 1b shows the FEM mesh during scratching. First, a normal force F_n is gradually applied to the indenter for 25 s, then, the scratch cycle takes place at constant scratch speed v_s.

3.5. Intrinsic response and model parameters

To investigate the intrinsic response of the polymer, single-element FEM compression simulations are performed and fitted to experimental data, obtained from Ref. [26]. The resulting reference spectra of

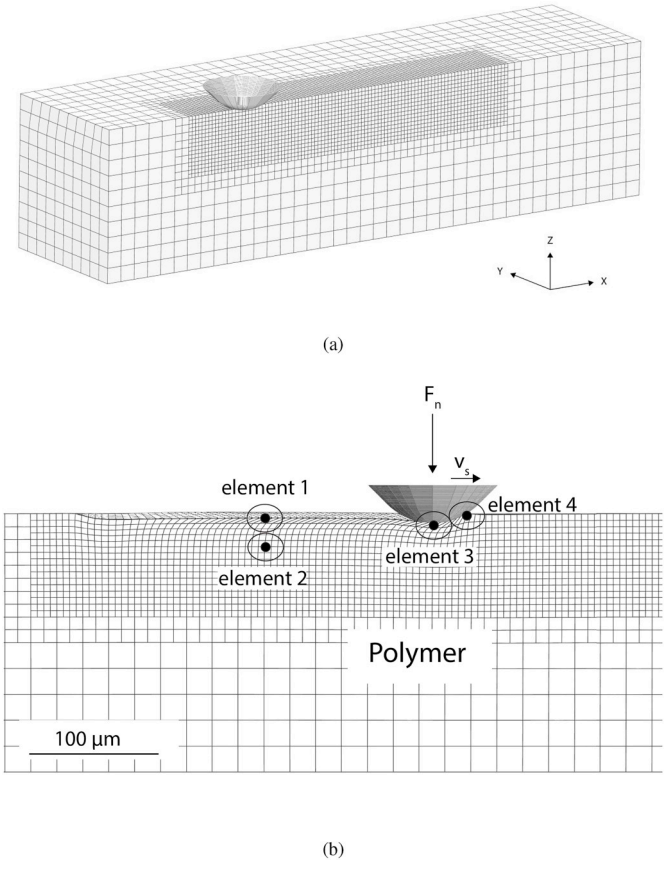

Fig. 1. FEM mesh of single-asperity scratch simulation; (a) 3D view before indention, (b) side view during scratching showing directions of applied normal force F_n and scratch velocity v_s on polymer surface. It also shows the location of the four elements considered to investigate the effect of the thermo-mechanical model, friction coefficient, and scratch speed on deformation kinetics.

α- and β-iPP are shown in Tables 1 and 2 in Appendix A. The thermodynamic state parameter of the material, S_a, is determined by using indentation simulations and fitting them to the experiments, similar to Ref. [14]. The material parameters for α- and β-iPP are obtained from Ref. [5] and tabulated in Tables 3 and 4 respectively. The pressure dependency parameter μ is determined from the compressive and tensile data obtained from Refs. [25,26]. The thermal parameters are adopted from Ref. [31], and presented in Table 5. It should be noted that V_1^* and V_2^* are the activation volumes for the primary and secondary molecular processes respectively, the same holds for the activation energies; ΔU_1 and ΔU_2.

The experimental intrinsic response of iPP is plotted in Fig. 2 by solid lines. The data show the response of α-iPP, Fig. 2a, and β-iPP, Fig. 2b. Due to the strain-rate dependence of the polymer, a higher yield stress is observed at higher strain rates for both phases. Fig. 3 shows the upper- and lower-yield stress for each phase versus the applied strain rate. The upper-yield stress displays a higher strain-rate dependence than the lower-yield stress. This implies that the upper-yield stress is controlled by a secondary molecular process in addition to the primary one, while only the primary process contributes to the kinetics of the lower-yield stress [5].

The simulation results are fitted to experimental data in order to obtain the model parameters as can be seen in Fig. 2. The first set of simulations "sim1" plotted by dotted lines clearly shows, at high strain rates, that the post-yield response is not captured by the model. This is due to the internal heat generation at these high rates. Due to high plastic deformation-rates, the material starts to soften as a result of heat dissipation. In addition, there is less time for conduction and convection of the generated heat. This leads to a significant effect on the post-yield response [5,30]. It should be noted that the existence of a secondary process controlling the upper-yield stress only manifests itself in a higher yield drop as the deformation rates increase within the assessed range of strain rates. The heat generation due to plastic deformation only appears at relatively high strain rates and alters the entire post-yield response. This explains the decrease in slope of the lower-yield stress at the highest strain rate, see Fig. 3. In this respect it is necessary to use a thermo-mechanically coupled model to accurately predict the post-yield response of the polymer. The other set of simulations "sim2" plotted by dashed lines shows the simulation results fitted to the experimental data after implementing the thermo-mechanically coupled model, Equations (16) and (17), and fitting the parameters Γ and k. Fig. 4 shows the temperature evolution due to plasticity-induced heating during the intrinsic simulations of iPP at different strain rates. The results reveal that the model is qualitatively able of determining the temperature evolution due to heat generation resulting from plastic deformation. Higher deformation rates result in more mechanical work dissipated into heat, and less time for cooling and temperature rises. The slight difference in the maximum temperatures between α-iPP and β-iPP can be related to the slightly higher yield stress of β-iPP at high strain rates.

4. Results and discussion

4.1. Influence of the thermo-mechanical model

The use of the thermo-mechanical model is proven to be necessary to capture the intrinsic response of the polymer at high strain rates. The model is expected to have a significant influence on the deformation kinetics during scratch. In order to show this influence, two single-asperity scratch simulations are performed using a mechanical model and a thermo-mechanical model respectively. In these simulations, indentation is first performed for 25 s where a normal load of $F_n = 200$ mN is gradually built-up, followed by constant-speed scratching of $v_s = 100$ μm/s for 250 μm. During this study, several elements are considered, see Fig. 1b. First, element 1 is an element on the surface of the polymer that is chosen to analyse the influence of the thermo-mechanical model on deformation kinetics. Steady-state response is

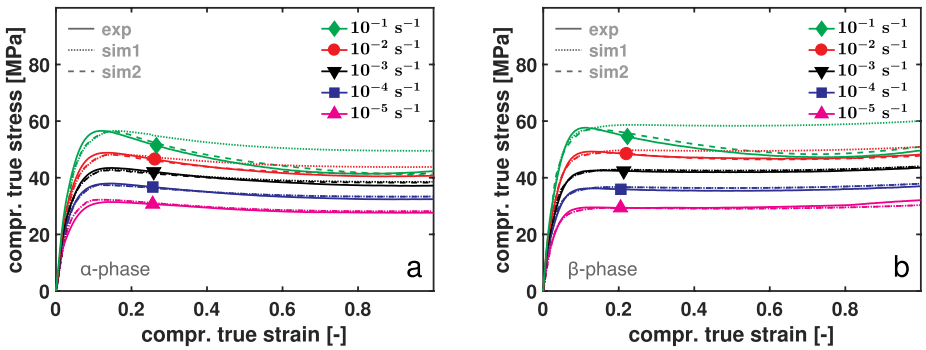

Fig. 2. Fitting uniaxial single-element compression simulation results to experimental data. Sim1 without considering heat generated due to plastic deformation. Sim2 using the thermo-mechanical coupled model. (a) α-iPP, (b) β-iPP.

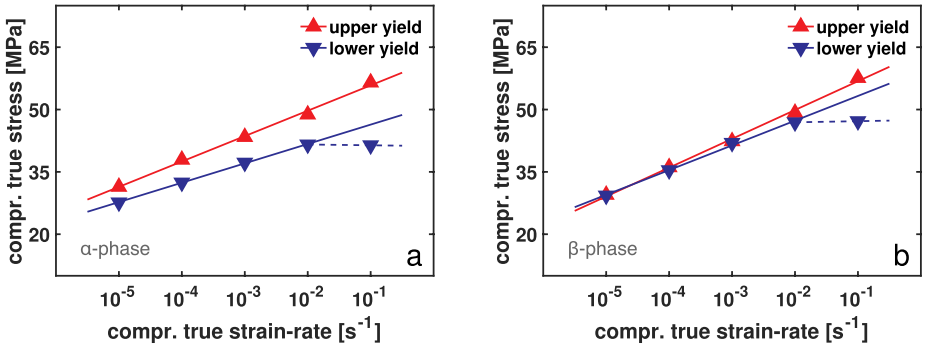

Fig. 3. Upper- and lower-yield stress values of iPP at different strain rates; (a) α-iPP, (b) β-iPP. Markers are data points, lines are data points fitting. The plastic heat generation leads to a decreased lower-yield slope at higher strain rates (dotted line).

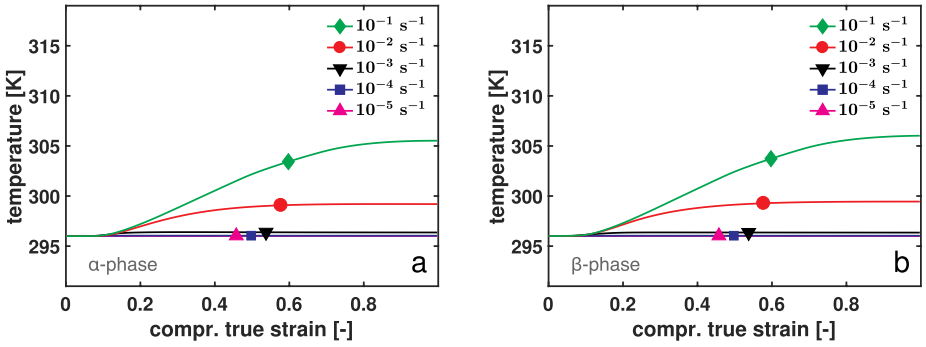

Fig. 4. Uniaxial single-element compression simulation results of temperature evolution due to heat generation resulting from plastic deformation of iPP at different strain rates; (a) α-iPP, (b) β-iPP.

already present when element 1 is reached. The analysis of element 1 only considers the scratch part which takes 2.5 s, while the indentation part which lasts for 25 s is not included. By definition, no mechanical work is dissipated into heat using the mechanical model, and therefore, no change in temperature can be observed, see Fig. 5a and b. Due to plastic heat generation using the thermo-mechanical model, material softens and deformation becomes slightly faster, see Fig. 5c. The equivalent stress is dependent on both deformation rate and temperature. Lower deformation rates and higher temperatures result in lower stresses. The values of deformation rate are almost the same in both cases. However, temperature is significantly higher when using the thermo-mechanical model. This leads to lower value of equivalent stress due to thermal softening, see Fig. 5d.

Heat is generated within each element of the FEM mesh according to plastic deformation-rates applied to this element. In order to show the temperature evolution along the mesh, next to element 1, three more elements located in different regions within the mesh, as shown in Fig. 1b, are considered. As these elements start to deform plastically, heat is generated within each element and the temperature rises, see Fig. 6. When the amount of heat conduction and convection become larger than heat generation, the temperature starts to slowly decrease. Element 2 experiences relatively small plastic deformation resulting in only a slight rise in temperature. It is clear from Fig. 6 that the trend of temperature evolution is proportional to that of the plastic strain $\bar{\gamma}_p$ evolution.

4.2. *Effect of friction on heat generation*

Friction is a crucial aspect in contact mechanics. Generally, more friction implies more adhesion between bodies in contact. This leads to more deformation in case of scratching, which is manifested in more distorted elements in simulations, compare Fig. 7a and b. Since we use a

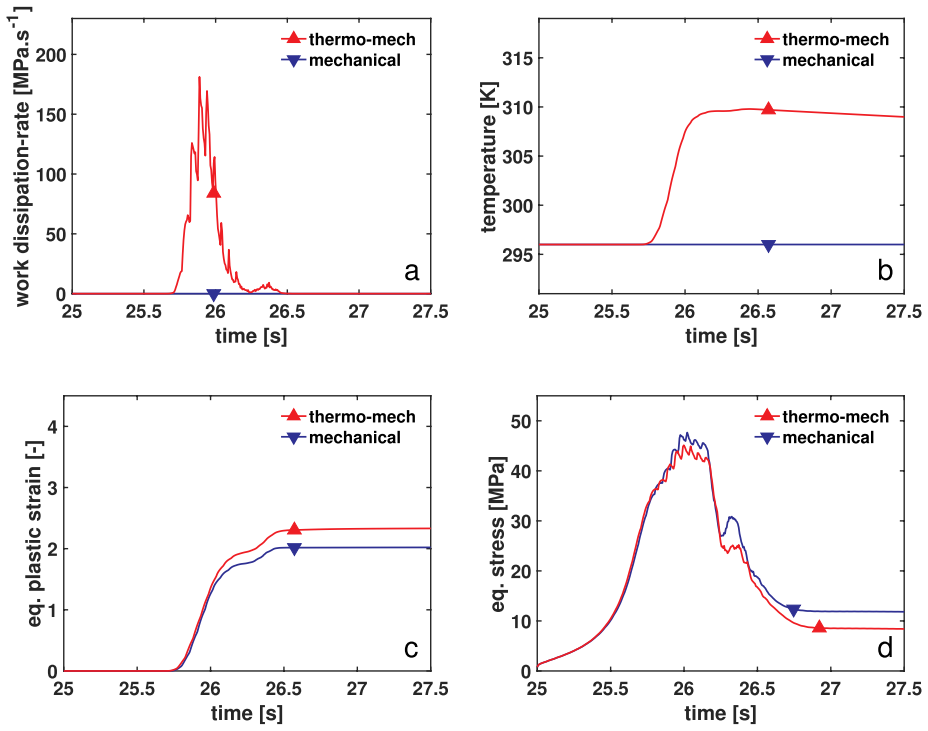

Fig. 5. The effect of using a thermo-mechanical model for scratch simulation and its influence on the deformation kinetics of element 1; (a) rate of mechanical work dissipated into heat, (b) the resulting rise in temperature, (c) the equivalent plastic strain, (d) the equivalent stress.

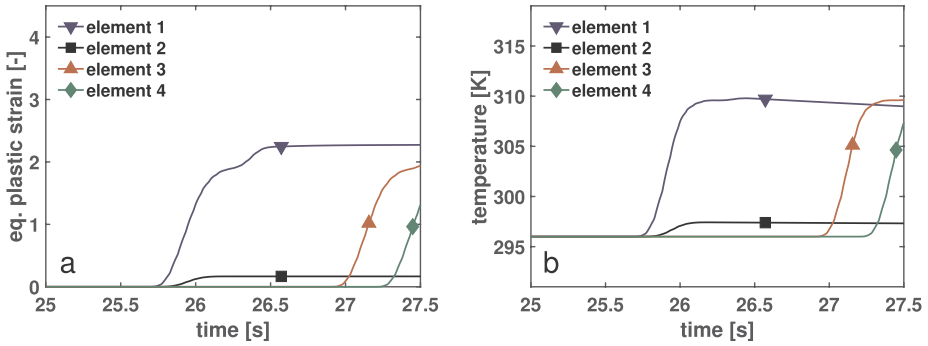

Fig. 6. (a) Plastic deformation of each element, (b) the resulting rise in temperature due to plastic deformation.

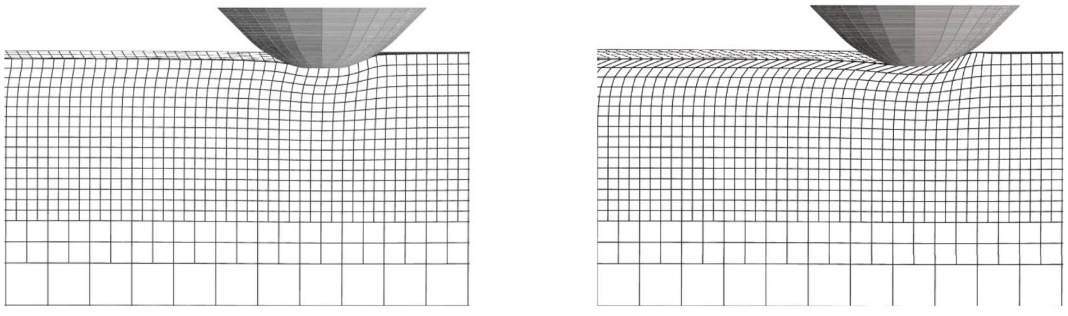

Fig. 7. Single-asperity scratch; (a) using friction coefficient $\mu_f = 0$, (b) using friction coefficient $\mu_f = 0.28$. Friction implies more polymer-tip adhesion, and thus, elements are more deformed.

thermo-mechanical model, more plastic deformation will lead to an increased heat generation. It should be noted however, that the we investigate how friction affects heat generation via deformation, and that heat generated due to friction itself is not accounted for in the used coulomb model. In order to investigate the influence of friction quantitatively, two single-asperity scratch simulations are performed. In the first one, the frictionless case is assumed, i.e. friction coefficient $\mu_f = 0.0$. In the second simulation a friction coefficient of $\mu_f = 0.28$ is used.

Both simulations are performed using the thermo-mechanical model, $F_n = 200$ mN, and $v_s = 100$ μm/s. Element 1 in Fig. 1b is chosen for this analysis. Frictional scratch leads to polymer-tip sticking, leading to more deformation and a higher deformation rate, see Fig. 8c. Therefore, more mechanical work is dissipated into heat, increasing the temperature of the polymer, see Fig. 8a and b. Fig. 8d shows the value of the equivalent stress. As mentioned earlier, the equivalent stress is dependent on both deformation rate and temperature. Before any plastic deformation of element 1, t = 25 s till t = 25.7 s, there is no heat generation, and thus, stress is only dependent on deformation rate (elastic) which is lower in the frictionless case, leading to a lower stress level. As plastic deformation takes place, t = 25.7 s till t = 26.5 s, and temperature starts to rise, the stress becomes dependent on both deformation rate and temperature. Finally, when the indenter continues scratching the surface and element 1 stops being deformed, t = 26.5 s till t = 27.5 s, stress becomes only dependent on temperature which is higher when friction is accounted for. Therefore, during this period the resulting equivalent stress from frictional scratch becomes lower than the frictionless case and reaches a steady-state value as the temperature reaches its steady-state value. From Fig. 8 it is observed that the value of mechanical work dissipated into heat is equal to the product of the equivalent stress and the equivalent plastic strain-rate multiplied by the percentage of mechanical work dissipated into heat parameter, Γ. This agrees with Equation (16).

4.3. Analysis of heat generation at various scratch velocities

As shown before, the equivalent plastic strain $\overline{\gamma}_p$ dictates the trend of temperature evolution. However, the time span in which this plastic strain takes place is critical. In another words, the faster the plastic deformation the higher the amount of mechanical work dissipated into heat according to Equation (16). In this respect, we test the influence of scratch velocities on heat generation. Three simulations are performed at $v_s = 1$ μm/s, 10 μm/s, and 100 μm/s. The applied load is $F_n = 200$ mN and the friction coefficient is $\mu_f = 0.28$. The scratch distance is 250 μm for all three simulations. Element 1 from Fig. 1b is again analysed for the three cases. Fig. 9a shows the evolution of the equivalent plastic strain along the entire scratch distance. Higher equivalent plastic strain is observed at lower scratch speeds due to the viscoelasticity of the polymer. However, at this lower speed, the time span to complete the entire scratch cycle is one order of magnitude lower than at $v_s = 10$ μm/s, and two orders of magnitude lower than at $v_s = 100$ μm/s. Thus, the plastic strain-rate is the lowest at this speed, leading to the lowest temperature increase observed, see Fig. 9b. Since there is enough time for conduction and convection of the generated heat, the temperature goes back to room temperature before the scratch cycle ends. As the scratch speed increases, plastic strain-rate also increases leading to higher maximum temperature generated, as seen in Fig. 9. It is clear how increasing the scratch speed by one order of magnitude has a significant effect on the temperature profile along the polymer surface (see Fig. 10).

4.4. Scratch and frictional response of α-iPP and β-iPP

Scratch tests are performed at three different scratch velocities; $v_s = 1$ μm/s 10 μm/s, and 100 μm/s, and at applied normal load $F_n = 200$ mN on both α-iPP and β-iPP. Indentation is first performed for 25 s, followed by a constant-speed scratch for 600 μm. The single-asperity scratch response for α-iPP and β-iPP is shown in Fig. 11. Fig. 11a and b show the value of indenter penetration into the polymer after indentation till it reaches the steady state for α-iPP and β-iPP respectively. Fig. 11c and d display the corresponding frictional response. One observation is the higher bumps in the beginning of the scratch cycle of α-iPP, which comes from the relatively low strain hardening that allows the tip to initially penetrate deeper before the frictional shear stress pushes the indenter back up and as a result the friction force drops. This observation is even more pronounced at the lowest speed due to the rate dependence of the polymer which allows more initial tip penetration. A second observation is the wavy response in case of α-iPP which is also related to the relatively low strain hardening that enhances the build-up of the bow wave in front of the tip, resulting in a more abrupt stick-slip cycle. Whereas in case of β-iPP, the higher strain hardening resists the build-up of the bow wave, resulting in

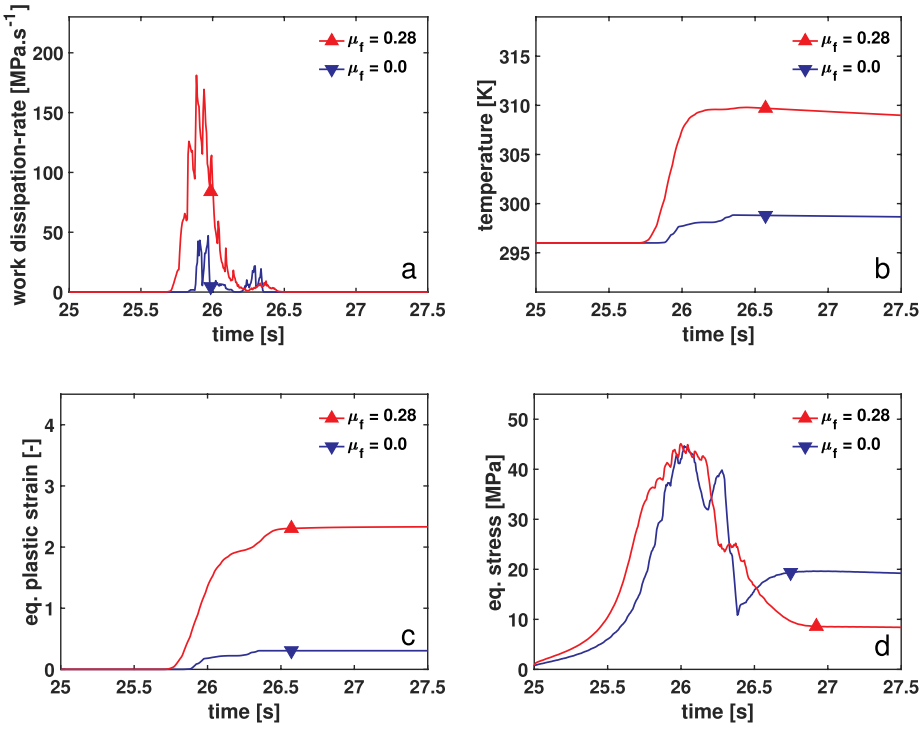

Fig. 8. The effect of friction during scratch simulation and its influence on the deformation kinetics of element 1; (a) rate of mechanical work dissipated into heat, (b) the resulting rise in temperature, (c) the equivalent plastic strain, (d) the equivalent stress.

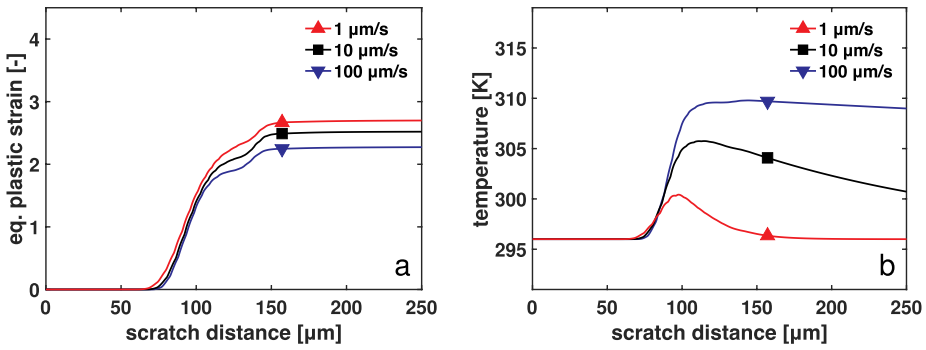

Fig. 9. (a) Plastic deformation of element 1 at $v_s = 1$, 10, and 100 μm/s (b) the resulting rise in temperature due to plastic deformation. More plastic deformation at the lowest speed due to the viscoelasticity of the polymer, however, more temperature rise at the highest speed due to higher plastic deformation-rates.

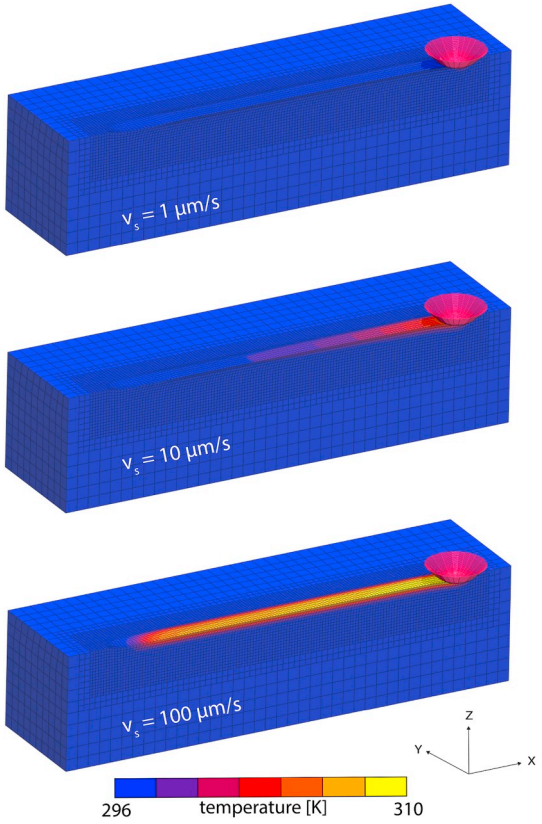

Fig. 10. FEM simulations showing temperature profiles along the surface of the polymer at $v_s = 1$, 10, 100 μm/s. At the lowest speed, lower deformation rates result in less temperature rise and more time for heat conduction and convection. The highest speed results in a lot of heat generation due to high plastic deformation-rates and less time for conduction and convection.

a smoother stick-slip cycle. Fig. 12a presents the values of the steady-state tip penetration into the polymer at each scratch speed. Fig. 12b displays the corresponding friction force values. The plots show more deformation-rate dependence for β-iPP which resembles its intrinsic response. As the scratch speed increases, the penetration depth and friction force values decrease at higher rate in case of β-iPP. This suggests that, in terms of friction and wear resistance, β-iPP performs better at higher scratch speeds.

4.5. Damage formation

The intrinsic response of the polymer has a crucial influence on its friction response. In this respect, it is necessary to quantitively investigate and link between the intrinsic response and the resulting friction response, and come up with a criterion for damage formation (i.e. initiation of wear). It has been reported that the so-called fish-scale damage pattern is the dominant damage mechanism that appears on the surface of polypropylene when scratched. This damage mechanism is controlled by the stick-slip phenomenon which occurs when the indenter experiences periodic changes in resistance. This periodic change comes from the periodic build-up of material in front of the tip, which in turn leads to the build-up of friction force to keep the constant velocity of the indenter. When the frictional shear stress is high enough, the indenter is suddenly pushed away, and slipping occurs. During the sticking cycle the material is plastically drawn along the scratch direction. This damage mechanism for polypropylene has been reported by many researchers [34–37]. Based on this, we select the equivalent plastic strain $\overline{\gamma}_p$ as a physical criterion to qualitatively assess and predict the formation of the fish-scale damage pattern. This criterion has been previously used to qualitatively assess damage formation on polymer and metal surfaces [46,47].

First, we are interested in investigating the influence of boundary conditions, i.e. normal load and scratch speed on damage formation. Fig. 13a shows the polymer surface of α-iPP after single-asperity scratch at various normal loads. At higher applied normal load, the tip penetrates more into the surface, creating more material build-up in front of the tip, making the stick-slip more abrupt and severe. This leads to material being more plastically drawn along the scratch direction. Fig. 13b displays the simulation results, in which the equivalent plastic strain $\overline{\gamma}_p$ contour profile is shown. Due to the increased normal load, more material is plastically deformed giving rise to the equivalent plastic strain. This is confirmed from the values of the width of the scratch which are quantitively comparable to the experimental values.

Due to rate dependency of the polymer, lowering scratch speed has an effect on the scratch response similar to that of a higher applied normal load. As scratch speed decreases, the indenter penetrates more into the polymer creating a more abrupt stick-slip cycles in which material experiences more plastic deformation, see Fig. 14.

The intrinsic response of the polymer is a critical factor, and plays a decisive role in its damage formation mechanism. Fig. 15a shows the polymer surface of α-iPP and β-iPP after single-asperity scratch. Fish-scale damage pattern is clearly visible in case of α-iPP. Simulation results, Fig. 15b, show that the maximum value of $\overline{\gamma}_p$ is significantly higher in case of α-iPP although penetration depth and friction force values at this speed are almost identical. However, looking at the intrinsic response of both phases, Fig. 15c, a significant difference in strain hardening is observed. Strain hardening is believed to be the reason behind damage formation differences between the two phases. A material with low strain hardening experiences more localized plastic deformation, and more material build-up, creating a more severe stick-slip cycle, leading to higher plastic deformation and fish-scale damage pattern becoming more visible.

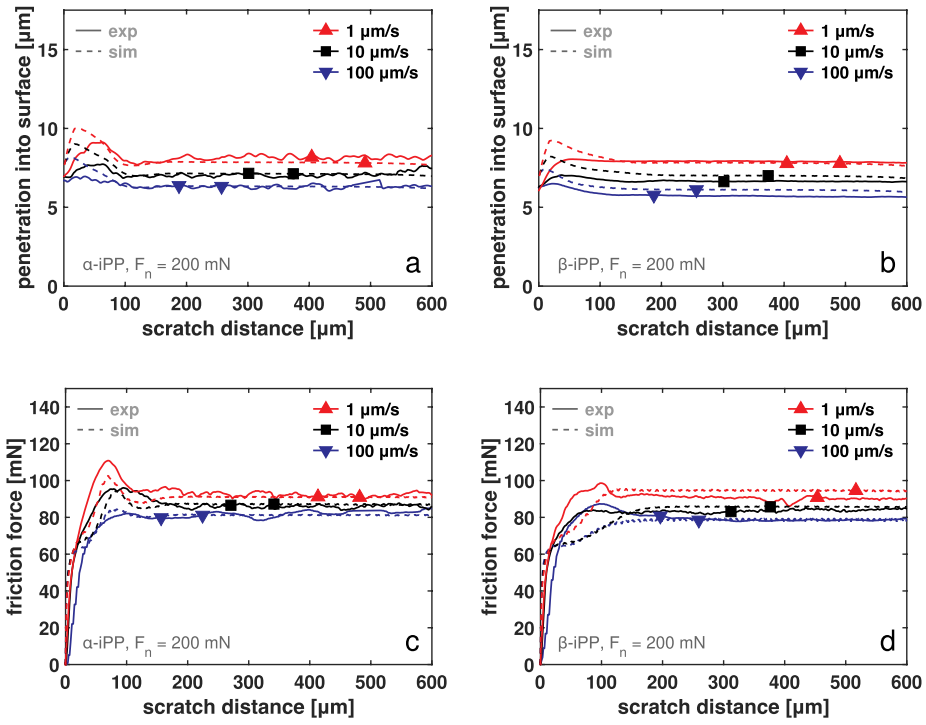

Fig. 11. Single-asperity scratch results of iPP; penetration into the surface versus sliding distance (a) α-iPP, (b) β-iPP, and friction force versus sliding distance (c) α-iPP, (d) β-iPP.

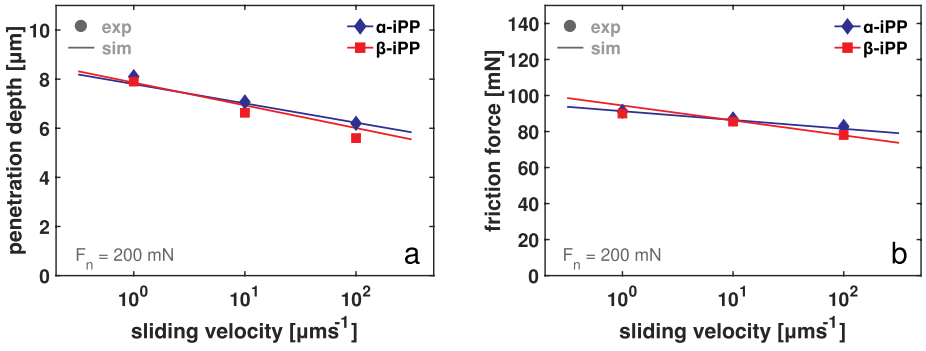

Fig. 12. (a) Steady-state penetration depth values at various scratch speeds, (b) steady-state friction force values at various scratch speeds. Data points are experiments, lines are fitting of simulation data points. The plots show more deformation-rate dependency for β-iPP which resembles its intrinsic reponse.

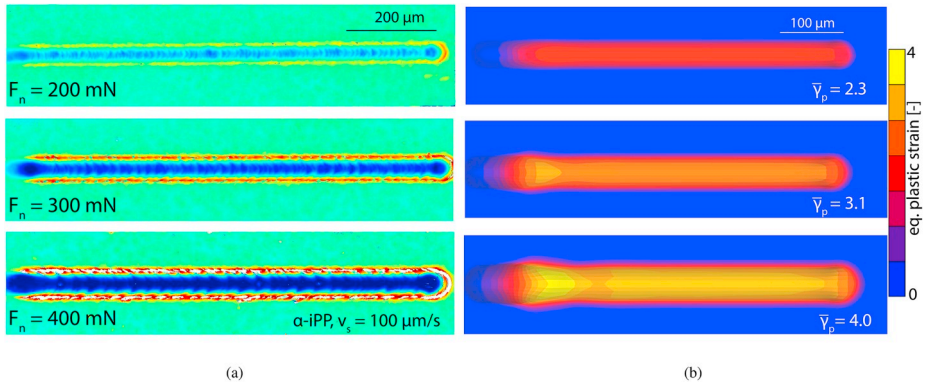

Fig. 13. Polymer surface of α-iPP after single-asperity scratch at various normal loads; (a) experimental, (b) simulations showing maximum value of $\bar{\gamma}_p$. Wider scratch profile appears at high normal loads. Higher equivalent plastic strain $\bar{\gamma}_p$ in simulations at high normal loads resembles the appearance of fish-scale damage pattern in experiments at these loads.

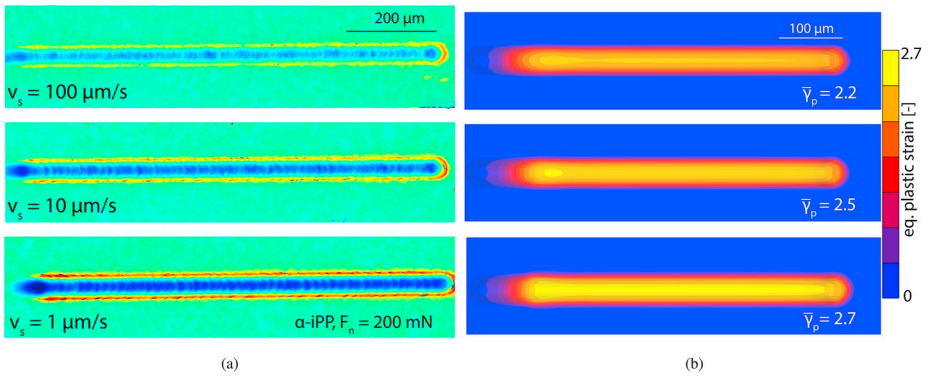

Fig. 14. Polymer surface of α-iPP after single-asperity scratch at various scratch speeds; (a) experimental, (b) simulations showing maximum value of $\bar{\gamma}_p$. Higher equivalent plastic strain $\bar{\gamma}_p$ appears in simulations at lower speeds due to the rate dependency of polymers. This explains the formation of fish-scale damage pattern at these speeds in experiments.

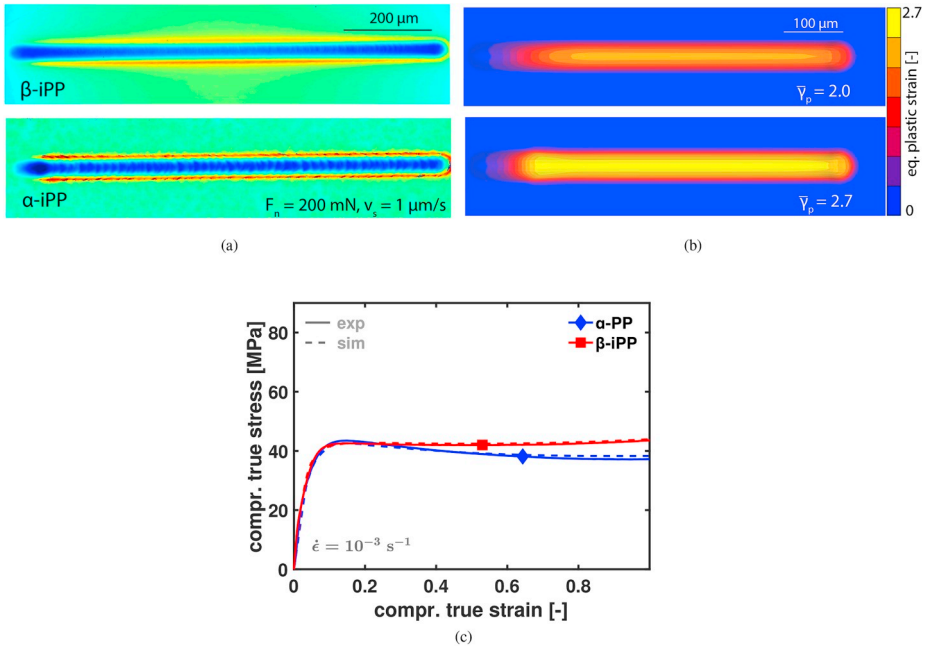

Fig. 15. Polymer surface of α-iPP and β-iPP after single-asperity scratch; (a) experimental, (b) simulations showing maximum value of $\bar{\gamma}_p$. Fish-scale damage pattern is clearly visible in case of α-iPP, and simulation results show higher equivalent plastic strain $\bar{\gamma}_p$ for α-iPP. (c) Intrinsic response of α-iPP and β-iPP show a significant difference in strain hardening, which is believed to be reason behind the damage formation differences between the two phases.

Due to the crystalline nature of iPP and other semi-crystalline polymers, material orientation has an effect on its intrinsic response [22,48]. During scratch, the material is oriented along the scratch direction. It is possible that the resulting material orientation has a critical role in damage formation. To test this hypothesis, the three principle strains of element 1 from Fig. 1b are obtained during scratching at a speed of 1 µm/s and 100 µm/s, see Fig. 16. Their values are comparable to the values of equivalent plastic strain $\bar{\gamma}_p$ in Fig. 14b. The equivalent plastic strain is only a summation of the magnitude of the plastic part of all principle strains. Scratching at 1 µm/s results in a 10% increase in all three principle directions when compared to scratching at 100 µm/s. Previous studies have shown that orientation, i.e. pre-stretch, results in less scratch depth and friction force and reduced damage [28,49]. However, in our case, the lowest scratch speed results in the highest penetration depth and friction force which leads to more apparent damage. This suggests that the viscoelasticity of the material, and not orientation, is the decisive factor in damage formation when comparing the scratch response at different scratch speeds. Similar observations hold when comparing different loads and phases. Although the current

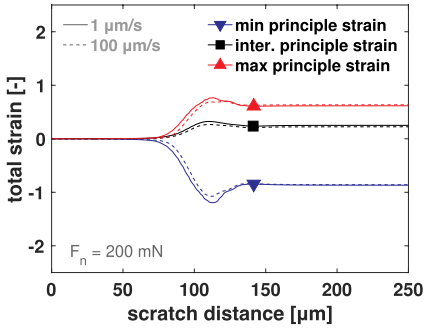

Fig. 16. The three principle strains of element 1 during scratching at a speed of 1 µm/s and 100 µm/s. Small difference in element stretching suggests that material orientation is not a critical factor in damage formation.

model does not account for material anisotropy, it is plausible for future work to include it in order to quantitatively investigate its effect on the scratch and frictional response. Senden et al. [48] used a 3D viscoelastic model based on Hill theory in order to predict the yield of drawn polypropylene tapes at various orientation angles with respect to the drawing direction. It is possible to simulate single-asperity scratch of an anisotropic polypropylene surface by implementing such a model in FEM.

5. Conclusions

A 3D elasto-viscoplastic constitutive model has been implemented in a FEM-framework to simulate a single-asperity scratch of two morphological structures; α- and β-iPP at different normal loads and scratch velocities. The physics-based thermo-mechanical model along with the experimental work formed the base of a hybrid experimental-numerical approach that was used to investigate the polymer scratch and frictional response based on its intrinsic response. From this study we conclude that:

1. The thermo-mechanical model is necessary to quantitatively predict the intrinsic response of the material especially at higher strain rates where heat is produced due the plastic deformation.
2. At higher scratch velocities, the polymer becomes more resistant to deformation due to its strain-rate dependence. This results in a lower scratch depth and friction force.
3. β-iPP exhibits a slightly higher strain-rate dependence than α-iPP. This leads to lower penetration depth and friction force at relatively high deformation rates. In this respect, β-iPP is a good choice for high-speed applications.
4. The stick-slip phenomenon is mainly responsible for the damage mechanism observed. During the sticking cycle the material is plastically drawn along the scratch direction creating the damage pattern. For this reason, the equivalent plastic strain $\overline{\gamma}_p$ has been chosen as a physical criterion to qualitatively assess and predict the formation of the fish-scale damage pattern.
5. The stick-slip phenomenon becomes more pronounced when the tip penetrates deep into the polymer, which introduces additional material build-up in front of the tip. A high normal load and low scratch speed lead to more tip penetration, thus, stick-slip becomes more severe. The material is more plastically deformed along the scratch direction and the fish-scale damage pattern is clearly observed.
6. A significant intrinsic difference between α-iPP and β-iPP is the strain hardening. In case of β-iPP the higher strain hardening resists the build-up of the bow wave in front of the tip resulting in less sticking and more slipping. Less material is plastically drawn along the scratch direction, preventing the formation of the fish-scale damage pattern. This makes β-iPP, again, a favourable choice over α-iPP for applications that require wear resistance.
7. The induced material orientation due to scratching is relatively low and does not have a significant role in damage formation.

Acknowledgements

This research forms part of the research programme of Dutch Polymer Institute (DPI), project 783t. The authors wish to thank DPI for their financial support.

Appendix A. Material parameters

Table 1
Reference spectrum of α-iPP.

Process 1	Mode	$\eta_{0,i,ref}$ [MPa.s]	G_i [MPa]
	1	1.6×10^8	110
	2	3.5×10^7	90
	3	2.3×10^6	70
	4	3.3×10^5	60
	5	3.3×10^4	40
	6	6.7×10^3	30
Process 2	**Mode**	$\eta_{0,i,ref}$ **[MPa.s]**	G_i **[MPa]**
	1	2.4×10^{-2}	80

Table 2
Reference spectrum β-iPP.

Process 1	Mode	$\eta_{0,i,ref}$ [MPa.s]	G_i [MPa]
	1	1.6×10^7	110
	2	3.5×10^6	90
	3	2.3×10^5	70
	4	3.3×10^4	60
	5	3.3×10^3	40
	6	6.7×10^2	30
Process 2	**Mode**	$\eta_{0,i,ref}$ **[MPa.s]**	G_i **[MPa]**
	1	2.4×10^{-2}	80

Table 3
Material parameters of α-iPP, adopted from Ref. [5].

G_r [MPa]	κ [MPa]	S_a [−]	μ [−]	V_1^* [nm^3]	V_2^* [nm^3]	ρ [gm/cm^3]	r_0 [−]	r_1 [−]	r_2 [−]
1.6	1650	5.0	0.12	3.10	3.0	0.90	0.95	2.0	−0.5

Table 4
Material parameters of β-iPP, adopted from Ref. [5].

G_r [MPa]	κ [MPa]	S_a [−]	μ [−]	V_1^* [nm^3]	V_2^* [nm^3]	ρ [gm/cm^3]	r_0 [−]	r_1 [−]	r_2 [−]
5.0	1650	5.0	0.18	2.90	3.0	0.90	0.95	2.0	−0.2

Table 5
Thermal parameters of α- and β-iPP, activation energy and specific heat capacity obtained from Ref. [31].

Γ [−]	k [MPa/K s]	ΔU_1 [kJ/mole]	ΔU_2 [kJ/mole]	c_p (kJ/kg K)
0.6	0.10	274	251	1.92

References

[1] Tervoort TA, Smit RJM, Brekelmans WAM, Govaert LE. A constitutive equation for the elasto-viscoplastic deformation of glassy polymers. Mech Time-Dependent Mater 1997;1(3):269–91.
[2] Govaert LE, Timmermans PHM, Brekelmans WAM. The influence of intrinsic strain softening on strain localization in polycarbonate: modeling and experimental validation. J. Eng. Mater. Technol. 2000;122(2):177–85.
[3] Klompen ETJ, Engels TAP, Govaert LE, Meijer HEH. Modeling of the postyield response of glassy polymers: influence of thermomechanical history. Macromolecules 2005;38(16):6997–7008.
[4] van Breemen LCA, Engels TAP, Pelletier CGN, Govaert LE, Den Toonder JMJ. Numerical simulation of flat-tip micro-indentation of glassy polymers: influence of loading speed and thermodynamic state. Philos Mag 2009;89(8):677–96.
[5] van Breemen LCA, Engels TAP, Klompen ETJ, Senden DJA, Govaert LE. Rate- and temperature-dependent strain softening in solid polymers. J Polym Sci B Polym Phys 2012;50(24):1757–71.
[6] Senden DJA, Krop S, van Dommelen JAW, Govaert LE. Rate- and temperature-dependent strain hardening of polycarbonate. J Polym Sci B Polym Phys 2012;50(24):1680–93.
[7] Arruda EM, Boyce MC. Evolution of plastic anisotropy in amorphous polymers during finite straining. Int J Plast 1993;9(6):697–720.
[8] Boyce MC, Parks DM, Argon AS. Large inelastic deformation of glassy polymers. part i: rate dependent constitutive model. Mech Mater 1988;7(1):15–33.
[9] Buckley CP, Jones DC. Glass-rubber constitutive model for amorphous polymers near the glass transition. Polymer 1995;36(17):3301–12.
[10] Buckley CP, Dooling PJ, Harding J, Ruiz C. Deformation of thermosetting resins at impact rates of strain. part 2: constitutive model with rejuvenation. J Mech Phys Solids 2004;52(10):2355–77.
[11] De Focatiis DSA, Embery J, Buckley CP. Large deformations in oriented polymer glasses: experimental study and a new glass-melt constitutive model. J Polym Sci B Polym Phys 2010;48(13):1449–63.
[12] Tervoort TA, Klompen ETJ, Govaert LE. A multi-mode approach to finite, three-dimensional, nonlinear viscoelastic behavior of polymer glasses. J Rheol 1996;40(5):779–97.
[13] van Breemen LCA, Klompen ETJ, Govaert LE, Meijer HEH. Extending the EGP constitutive model for polymer glasses to multiple relaxation times. J Mech Phys Solids 2011;59(10):2191–207.
[14] van Breemen LCA, Govaert LE, Meijer HEH. Scratching polycarbonate: a quantitative model. Wear 2012;274–275:238–47.
[15] Krop S, Meijer HEH, van Breemen LCA. Finite element modeling and experimental validation of single-asperity sliding friction of diamond against reinforced and non-filled polycarbonate. Wear 2016;356–357:77–85.
[16] Oral E, Wannomae KK, Hawkins N, Harris WH, Muratoglu OK. α-tocopherol-doped irradiated UHMWPE for high fatigue resistance and low wear. Biomaterials 2004;25(24):5515–22.
[17] Muratoglu OK, Bragdon CR, O'Connor DO, Jasty M, Harris WH, Rizwan G, McGarry F. Unified wear model for highly crosslinked ultra-high molecular weight polyethylenes (UHMWPE). Biomaterials 1999;20(16):1463–70.
[18] Renò F, Cannas M. UHMWPE and vitamin E bioactivity: an emerging perspective. Biomaterials 2006;27(16):3039–43.
[19] Atwood SA, van Citters DW, Patten EW, Furmanski J, Ries MD, Pruitt LA. Tradeoffs amongst fatigue, wear, and oxidation resistance of cross-linked ultra-high molecular weight polyethylene. J Mech Behav Biomed Mater 2011;4(7):1033–45.
[20] Fu J, Ghali BW, Lozynsky AJ, Oral E, Muratoglu OK. Wear resistant UHMWPE with high toughness by high temperature melting and subsequent radiation cross-linking. Polymer 2011;52(4):1155–62.
[21] Keller A, Machin MJ. Oriented crystallization in polymers. J Macromol Sci, Part B 1967;1(1):41–91.
[22] van Erp TB, Reynolds CT, Peijs T, van Dommelen JAW, Govaert LE. Prediction of yield and long-term failure of oriented polypropylene: kinetics and anisotropy. J Polym Sci B Polym Phys 2009;47(20):2026–35.
[23] van Erp TB, Cavallo D, Peters GWM, Govaert LE. Rate-, temperature-, and structure-dependent yield kinetics of isotactic polypropylene. J Polym Sci B Polym Phys 2012;50(20):1438–51.
[24] Caelers HJM, Govaert LE, Peters GWM. The prediction of mechanical performance of isotactic polypropylene on the basis of processing conditions. Polymer 2016;83:116–28.
[25] H. J. M. Caelers, E. M. Troisi, L. E. Govaert, G. W. M. Peters, Deformation-induced phase transitions in iPP polymorphs, Polymers 9 (10).
[26] Caelers HJM, Parodi E, Cavallo D, Peters GWM, Govaert LE. Deformation and failure kinetics of iPP polymorphs. J Polym Sci B Polym Phys 2017;55(9):729–47.
[27] Gao WM, Wang L, Coffey JK, Daver F. Finite element simulation of scratch on polypropylene panels. Mater Des 2018;140:400–8.
[28] Looijmans SFSP, Anderson PD, van Breemen LCA. Contact mechanics of isotactic polypropylene: effect of pre-stretch on the frictional response. Wear 2018;398:183–90.
[29] Adams GW, Farris RJ. Latent energy of deformation of bisphenol a polycarbonate. J Polym Sci B Polym Phys 1988;26(2):433–45.
[30] Boyce MC, Montagut EL, Argon AS. The effects of thermomechanical coupling on the cold drawing process of glassy polymers. Polym Eng Sci 1992;32(16):1073–85.
[31] Klompen ETJ. Mechanical properties of solid polymers : constitutive modelling of long and short term behaviour. Ph.D. thesis. Department of Mechanical Engineering; 2005.
[32] van Melick HGH, Govaert LE, Meijer HEH. Localisation phenomena in glassy polymers: influence of thermal and mechanical history. Polymer 2003;44(12):3579–91.
[33] Meijer HEH, Govaert LE. Mechanical performance of polymer systems: the relation between structure and properties. Prog Polym Sci 2005;30(8–9):915–38.
[34] Jiang H, Browning R, Sue H-J. Understanding of scratch-induced damage mechanisms in polymers. Polymer 2009;50(16):4056–65.
[35] Xiang C, Sue H-J, Chu J, Coleman B. Scratch behavior and material property relationship in polymers. J Polym Sci B Polym Phys 2001;39(1):47–59.
[36] Wong M, Lim GT, Moyse A, Reddy JN, Sue H-J. A new test methodology for evaluating scratch resistance of polymers. Wear 2004;256(11–12):1214–27.
[37] Jiang H, Cheng Q, Jiang C, Zhang J, Yonghua L. Effect of stick-slip on the scratch performance of polypropylene. Tribol Int 2015;91:1–5.
[38] Duckett RA, Rabinowitz S, Ward IM. The strain-rate, temperature and pressure dependence of yield of isotropic poly (methylmethacrylate) and poly (ethylene terephthalate). J Mater Sci 1970;5(10):909–15.
[39] Rabinowitz S, Ward IM, Parry JSC. The effect of hydrostatic pressure on the shear yield behaviour of polymers. J Mater Sci 1970;5(1):29–39.
[40] Duckett RA, Goswami BC, Smith LSA, Ward AM, M I, Zihlif. The yielding and crazing behaviour of polycarbonate in torsion under superposed hydrostatic pressure. Br Polym J 1978;10(1):11–6.
[41] Ree T, Eyring H. Theory of non-Newtonian flow. i. solid plastic system. J Appl Phys 1955;26(7):793–800.
[42] Roetling JA. Yield stress behaviour of isotactic polypropylene. Polymer 1966;7(7):303–6.
[43] Lee EH. Elastic-plastic deformation at finite strains. J Appl Mech 1969;36(1):1–6.
[44] Besseling J, van der Giessen E. Mathematical modeling of inelastic deformation, vol. 5. CRC Press; 1994.
[45] Ziegler H. An introduction to thermomechanics, vol. 21. Elsevier; 2012.
[46] Pelletier H, Gauthier C, Schirrer R. Influence of the friction coefficient on the contact geometry during scratch onto amorphous polymers. Wear 2010;268(9–10):1157–69.

[47] Bellemare SC, Dao M, Suresh S. Effects of mechanical properties and surface friction on elasto-plastic sliding contact. Mech Mater 2008;40(4–5):206–19.
[48] Senden DJA, Peters GWM, Govaert LE, van Dommelen JAW. Anisotropic yielding of injection molded polyethylene: experiments and modeling. Polymer 2013;54 (21):5899–908.
[49] Looijmans SFSP, Anderson PD, van Breemen LCA. Contact mechanics of high-density polyethylene: effect of pre-stretch on the frictional response and the onset of wear. Wear 2018;410:142–8.